AN ABSTRACT OF THE THESIS OF

Cade W. Trotter for the degree of Master of Science in Electrical Engineering and Computer Science presented on June 9, 2021.

Title: Indoor Free-Space Optical Communication Enhanced by Dynamic Optical Beam Control

Abstract approved:

_____

Alan X. Wang

This work expands the field of indoor free-space optical communication by introducing novel techniques in short range optical communication. The increasing need for high bandwidth communication necessitates the transition to optical frequencies with hundreds of terahertz worth of unregulated bandwidth. Optical communication offers an inherent security advantage over traditional communications methods by utilizing line-of-sight data transmission. First, we experimentally demonstrate a 1Gb/s, dynamically adjustable, all-optical communication system capable of securely locating and transmitting data to a static user in the field of view (FOV). Second, we propose and lay the foundation for a 10Gb/s, optical communication system capable of tracking and sending data to a user in the field of view.

Indoor Free-Space Optical Communication Enhanced by Dynamic Optical Beam
Control

by
Cade W. Trotter

A THESIS

submitted to

Oregon State University

in partial fulfillment of
the requirements for the
degree of

Master of Science

Presented June 9, 2021
Commencement June 2022

<u>Master of Science</u> thesis of <u>Cade W. Trotter</u> presented on <u>June 9, 2021</u>

APPROVED:

_____

Major Professor, representing Electrical and Computer Engineering

_____

Head of the School of Electrical Engineering and Computer Science

_____

Dean of the Graduate School

I understand that my thesis will become part of the permanent collection of Oregon State University libraries. My signature below authorizes release of my thesis to any reader upon request.

_____

Cade W. Trotter, Author

ACKNOWLEDGEMENTS

I would like to thank my advisor, Dr. Alan X. Wang, for his continual support and guidance over the last two years. Without his mentorship, the success of this project would not be possible.

I would like to thank the rest of my peers and mentors that made this all possible: Luc Bouchard, Dr. Spencer Liverman, Hayden Bialek, Dr. Arun Natarajan, and Dr. Thinh Nguyen.

I would like to thank my family and friends for their support these last few years.

Finally, I would like to thank my wife, Abby, for her unlimited patience and support.

TABLE OF CONTENTS

LIST OF FIGURES

CHAPTER 1: INTRODUCTION

The world's ever-growing need for higher bandwidth has spurred an evolution in optical communications systems over the past several decades. Ranging from guided wave optical communications systems to free-space optical (FSO) communications the field has continually risen to the challenge of increasing data requirements.

The field of guided wave optical communications describes the use of media to confine the propagation of light waves to transmit and receive signals. This confinement is made possible by the phenomenon of total internal reflection (TIR). TIR is present when light from one medium interacts with the boundary of a medium with a lower index of refraction. If this interaction satisfies the criteria of exceeding the critical angle, then total internal reflection occurs. Optical fibers rely on the use of TIR to guide modulated signals of light distances of kilometers with minimal degradation [1]. While optical fibers have revolutionized medium and long-haul data transmission, they are not always the optimal solution for short-haul applications.

In recent years free-space optical communication systems have demonstrated remarkable maturation in all distances of communication [2]. In particular, FSO systems have filled the role of the short-range, highly secure, data requirements. The use of adaptive optics, low-cost lasers, and high-bandwidth receivers has substantially improved the performance of optical communications [3].

1.1 Modulation

The process of transmitting information via optical communications allows for many advantages, yet it relies on the same fundamental principle of representing data as a "1" or a "0". While light can be modulated both in phase, and in amplitude, the most ubiquitous methods often fall under amplitude modulation. Amplitude modulation in the context of optical communication comes in the form of representing a "0" with a low or nearly zero optical power level, and a "1" with a higher optical power level. The large frequencies provided in the infrared and visible spectrum allow for exceedingly larger modulation frequencies than that of traditional radio frequency (RF) communication. In the context of the work provided in this thesis, all modulation is performed via amplitude modulation, more specifically non-return-to-zero on-off-keying (NRZ-OOK). The key differences between NRZ-OOK and return-to-zero on-off-keying (RZ-OOK) is that when representing a bit of data NRZ is structured such that there is no need to buffer any modulation with a zero after every transmitted bit, thus allowing for NRZ-OOK to have twice the bit rate of RZ-OOK.

1.2 Light Sources

The process of modulating light in the context of this work is by means of direct modulation. Direct modulation is the process by which light is modulated in intensity at its creation rather than by means of an external modulation in which light is generated and attenuated for purposes of modulation. Direct modulation is straightforward where

light is generated with a direct proportionality to current as in diode lasers. The two key transmitters in this manuscript are: a vertical cavity surface emitting laser (VCSEL) diode transmitter, and a small-form-factor pluggable (SFP) transceiver. VCSEL diodes offer unique advantages in both their cost due easy fabrication, and their low power consumption because of low threshold currents. Where off-the-shelf SFP transceivers allow for high-speed modulation and ease of use due to their ubiquity in telecom applications.

1.3 Photodiodes

The two most ubiquitous photodiodes in the application of optical communication are PIN photodiodes and avalanche photodiodes (APD). The tradeoffs in use cases are a result of sensitivity, noise, and power consumption. Avalanche photodiodes operate with large reverse bias voltages that allow for impact ionization to occur which accounts for the internal gain realized by these devices. Traditional PIN photodiodes similarly utilize the photoelectric effect, however there is no internal gain and the output signal must be amplified for a PIN receiver to have gain. The simplicity of PIN photodiodes often allows for applications in FSO communications due to their superior noise figures as compared to APDs. For this purpose, all photodiodes used in this work fall under the category of PIN photodiodes.

1.4 Adaptive Optics

Advancements adaptive optic technology has stimulated novel techniques in

free-space optical communication. Particularly, advancements in the field of beam steering and beam shaping have allowed for innovation in aspects of FSO communications ranging from user location techniques to optimization of signal-to-noise ratio in adaptive optics systems. While there are many adaptive optic techniques, four key technologies are frequently utilized: spatial light modulators (SLM), acousto-optics (AO), galvanometer mirrors, and micro-electrical-mechanical systems (MEMS).

- SLM technologies make use of optically anisotropic materials by using an electric field to manipulate the properties of incident light.

- AO technologies control the index of refraction of a material by inducing a strain wave through the material, thus diffracting the beam.

- Galvanometer mirrors are enabled by motorized mirrors and often have a large current draw.

- MEMS technologies in the context of beam steering and shaping operate using electrostatically actuating components to move optically reflective surfaces.

1.5 Thesis Organization

In Chapter 2 of this thesis, a dynamically controlled beam steering and shaping free-space optical communication system is proposed and demonstrated. In that system, 1 Gb/s link is created to a user in a known field of view (FOV) by the utilization of beam steering and beam shaping techniques to locate a receiver

supplemented with a toroidal shaped retroreflector. The system offers high-speed communication, and a secure link to the user.

In Chapter 3 of this thesis, a free-space optical communication system enabled by user tracking is proposed, and the experimental groundwork is established. The system offers a 10Gb/s link to a user and supports user movement in the FOV by employing a tracking algorithm guided by retroreflector based optical feedback. This system will provide a high-speed, robust link.

In Chapter 4, a summary of the of overall work is included.

CHAPTER 2: Dynamic, 1Gb/s, Free-Space Optical Communication Enhanced by Static User Location

2.1 Background

Due to the unregulated operational spectra, indoor free-space optical (FSO) communication systems are becoming an increasingly competitive alternative to radio frequency (RF) communication [4-6]. However, existing FSO systems lack the flexibility required for robust, high-speed, indoor wireless communication. Current indoor FSO implementations use direct line-of-sight (LOS) transmission [7-9, broadcast data transmission [10-11], a combination of both [12] or a synergic integration with an existing WiFi system [13-14]. While LOS transmission offers advantages in data security and power efficiency and can achieve data rates up to tens of gigabits per second (Gb/s), it is intrinsically limited to point-to-point connections and cannot support mobile users. On the other hand, broadcast data transmission allows users to move freely, but the received optical power is low, limiting data rates to hundreds of megabits per second (Mb/s). While the received power can be boosted with high power light-emitting diodes (LEDs) such as white LEDs [15-16] or high-power laser diodes [17-18], these optical transmitters are very power hungry and as such are difficult to be used for indoor FSO communications. On the receiver side, complex light concentration devices such as focusing lenses [18] or parabolic reflectors [19] can also increase the optical power at the receiving end of a broadcast

transmission, but they do so at the expense of user convenience.

Interestingly, extensive work has been done on long-distance FSO links such as inter-satellite, ground-to-satellite, and ship-to air communication [20-23]. In these applications, rapidly locking a target at long distance and transmitting data in the presence of atmospheric turbulence requires sophisticated acquisition system based on adaptive optics [24]. For example, in the case of a research article space optical communication, pointing accuracy was accomplished using a hybrid pointing architecture using inertial sensors, celestial reference and an uplink beacon [25-26]. Such a bulky, expensive beam controlling system designed for long distance FSO is not practical for indoor wireless communication. However, the concept of integrating beam steering and beam shaping modules with FSO links is inspiring to solve the challenges of indoor wireless communication and a reconfigurable optical wireless connection was proposed by N.A. Riza in 1999 [27]. In recent years, FSO links using optical beam steering schemes, including optical gratings [28-29], optical phased arrays (OPAs) [30], and MEMS mirrors [31] have been demonstrated conceptually to implement short-distance, predetermined, point-to-point optical transmission. However, a beam steering scheme alone without beam shaping cannot meet the bandwidth, power efficiency, data security, and areal coverage requirements of a robust wireless communication system due to the lack of control of the beam spot size. A holistic, cost-effective, agile beam controlling system is required to handle the complex scenarios of indoor wireless communication. Recently, FSO systems with beam-

shaping capabilities were also reported to provide another dimension of control of the laser beam [31-32]. In addition, there is another essential requirement to have a feedback mechanism for the transmitter to locate the receiver. Such feedback mechanism has been implemented by a camera [33], or a hybrid RF feedback [14], or bright LED broadcasting [34], or 60GHz antenna pattern nulling [35], or retroreflector optical feedback [36]. However, each feedback mechanism brings some system-level tradeoffs in terms of additional power consumption and complexity.

In this article, we present an agile indoor FSO communication system by combining beam steering and beam forming devices with passive optical beacons. The system demonstrated reliable, rapid, accurate, and all-optical user location at arbitrary positions within a large field-of-view (FOV) and in the meanwhile, achieved enhanced optical power at the receiver end. The optical transmitter and receiver of the FSO system were built using off-the-shelf products, including a vertical cavity surface emitting laser (VCSEL) diode and p-i-n photodiode with ball lens. As the core of the dynamic FSO link, the beam steering and beam shaping module consists of a pair of galvo-mirrors for two-dimensional (2-D) beam steering, and a deformable Micro Electro-Mechanical System (MEMS) mirror that can adjust the beam spot size. Although MEMS steering mirrors as mentioned in [31] can provide higher steering speed and consumes lower power, the relatively small size of off-the-shelf MEMS scanning mirrors cannot reflect the laser spot controlled by the deformable mirror with high efficiency, especially when the laser beam has a large divergent angle. Therefore,

galvo-mirrors were selected as the feasible engineering solution. To provide rapid feedback of the user location, the ring-shaped retroreflector around the optical receiver serves as a passive beacon and an optical sensor array consisting of three domed-lens photodetectors is integrated with the optical transmitter to receive the beacon signals. Such all-optical feedback mechanism based on retroreflector and optical sensor array allows the transmitter to find the receiver's position without an active feedback mechanism, and the optical sensor array provides a high-sensitively, large area detector that can serve as both a beacon detection sensor and a medium speed optical receiver for bidirectional communication to be implemented in the future. In order to enable highly secure, power-efficient LOS optical link, we developed a three-step user-scanning algorithm to achieve millimeter-scale location accuracy at a distance of more than three meters within an FOV of $\pm 11.25°$ in the vertical direction and $\pm 18.75°$ in the horizontal direction. Due to the superior beam controlling system, we were able to demonstrate 1Gb/s data rate with a bit error rate (BER) below 4×10^{-7} using an 850 nm wavelength VCSEL diode with only 2mW output power. Such low output laser power can meet the requirement of the International Electro-technical Commission (*IEC*) *standard 60825-1* on eye safety by ensuring the safety even when the eyes are in direct contact with the laser spot. If the low power transmitter is combined with a simple communication protocol to monitor the reflected beacon signals from the retroreflector, we will be able to further minimize accidental eye exposure, which is superior to traditional high-power visible light LED FSO communications.

2.2 System Architecture

As illustrated in Figure 2.1, the FSO system presented in this paper consists of three primary components: the transmitter module, the beam controlling module, and the receiver module. The transmitter module uses a collimated VCSEL diode to transmit non-return-to-zero on-off keying (NRZ-OOK) modulated optical signals at data rates up to 1 Gb/s. The beam controlling module uses beam steering and beam shaping devices to direct the transmitter beam toward the user, and it uses an optical sensor array to detect the optical reflection from the user. The receiver module, referred to as the "user" in later sections, combines a ring-shaped retroreflector with a high-speed optical receiver. The retroreflector serves as a passive beacon that the beam controlling module leverages to find the user and is cut from a roll of 3M 3430 white micro prismatic sheeting reflective tape. The optical receiver integrates a trans-impedance amplifier (TIA) and a clock-data recovery (CDR) circuit. The output signals are monitored by a bit error rate tester (BERT) oscilloscope. A user location acquisition algorithm using a Python program drives the beam controlling module to precisely locate the user and establish a high speed, highly secure optical link in approximately 1.16 seconds.
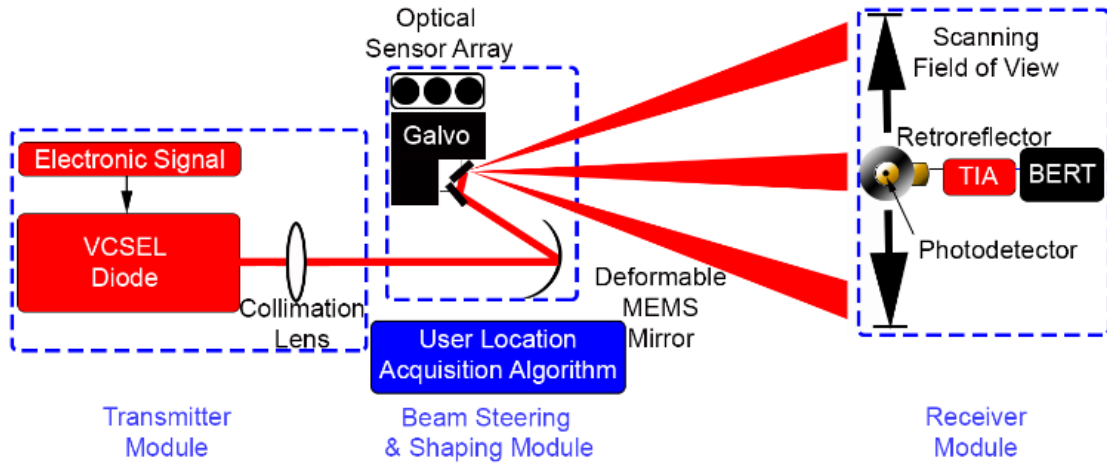
Figure 2.1: Schematic of the 850nm user location FSO system consisting of a transmitter module, a beam steering and beam shaping module controlled by a user location acquisition algorithm, and receiver module with a retroreflector as the passive beacon.

2.2.1 Transmitter Module

The transmitter module is shown Figure 2.2 (a). A direct modulation VCSEL diode from Finisar HFE4080-321 with a center wavelength at 850nm is selected as the transmitter light source. An enhancement-mode pseudomorphic high-electron-mobility transistor (E-pHEMT) is used to drive the VCSEL due to its high modulation speeds of 1.25 Gb/s and large drain current. A bias tee is also used to set the DC current through the VCSEL. The laser transmitter operates on an efficient 58mW power consumption. An aspheric lens is mounted to collimate the light emitted from the transmitter module.

2.2.2 Beam Controlling Module

The beam controlling module is also shown in Figure 2.2 (a). The beam shaping capability is provided by a deformable MEMS mirror from Revibro Optics. This device suspends a circular reflective membrane anchored around its edges above an electrostatic actuator. When no voltage is applied, the MEMS device forms a flat mirror with an infinitely long focal length, meaning the collimated light from the optical transmitter maintains its collimation and propagates with the minimum divergence angle of $0.2°$. As the applied voltage increases, the center of the reflective membrane is pulled downward, forming a concave mirror that causes the collimated beam to diverge. Under maximum deflection, the MEMS device forms a mirror with a focal length of 67mm. The Revibro deformable MEMS mirror changes focal lengths with a settling time of just 150µs, dynamically controlling the spot size of the transmission beam incident on the receiver. As it can dynamically adjust the beam spot size to optimize the optical power density, beam shaping is a critical capability for rapidly scanning and locating a user in the FOV and also makes it possible to optimize power efficiency, user mobility, and data security. Beam steering is implemented using a set of perpendicularly mounted galvo mirrors. Galvo mirror scanner is a mature technology with relatively high speed and precision. Additionally, galvo mirrors have a significantly larger reflective area than MEMS mirrors, which can provide excellent collimation for the laser beam. A two-dimensional galvo mirror steering system from Thorlabs (GVSM002) is selected to reduce rounding effects on scan pattern corners. In

our system, each mirror can steer the transmitted beam across a FOV of $\pm17°$ in the horizontal direction and $\pm25°$ in the vertical direction, both at a scanning rate of 100Hz. Within each FOV scanning, the angular resolution can be as fine as $0.0008°$ and the scanning step can be as fast as 2 kHz. To receive the weak feedback signals from the passive beacon at the receiver, a high-sensitivity optical sensor array is integrated with the beam control module, which faces outwardly toward the direction of the transmitter's FOV. The optical sensor array draws 520mW of power and can detect the reflected optical signals from the retroreflector with the receiver. To increase the sensitivity, the optical sensor array sums the photocurrents generated by three large area Hamamatsu photodiodes S6968-01 with domed lenses. The domed lenses are made of epoxy that filters out visible wavelengths. This epoxy becomes opaque to wavelengths shorter than 800nm. For longer wavelengths, the responsivity curve of the silicon photodiode drops off at 1000nm. The resulting effective spectral bandwidth of the optical receiver is 200nm with a peak responsivity at 870nm.

2.2.3 Receiver Module

The receiver module, which is shown in Figure 2.2 (b), implements a saturated data path including a high-speed silicon photodiode from Hamamatsu, a TIA, a limiting amplifier, and a CDR circuit, all integrated on a printed circuit board. The receiver module draws 360mW of power and can detect encoded optical signal using NRZ-

OOK modulation format up to a data rate of 1 Gb/s. in the demonstrated FSO system. The photodiode selected for this design is a Hamamatsu S5973-01 silicon PIN diode with a 0.4 mm diameter. The photodiode sets the bandwidth limit of the system with a cutoff frequency of 1 GHz and is packaged with a 1.5 mm diameter ball lens. Both the optical sensor and the receiver select components and materials to bring the total area to a few square centimeters while keeping the overall weight down. To acquire the user location data, a ring-shaped retroreflector is placed around the photodiode to reflect probing signals from the transmitter. The ring shape of the retroreflector symmetrically reflects the optical beam regardless of scanning direction. Similar techniques have been shown in [36] with the use of passive optical location. However, our use of dynamically adjusting beam shaping has done well to compliment this technology by decreasing acquisition time by an order of magnitude. The photodetector is placed in a hole in the center of the retroreflector, providing a reflection contrast that improves the photodetector location estimate to millimeter scale.
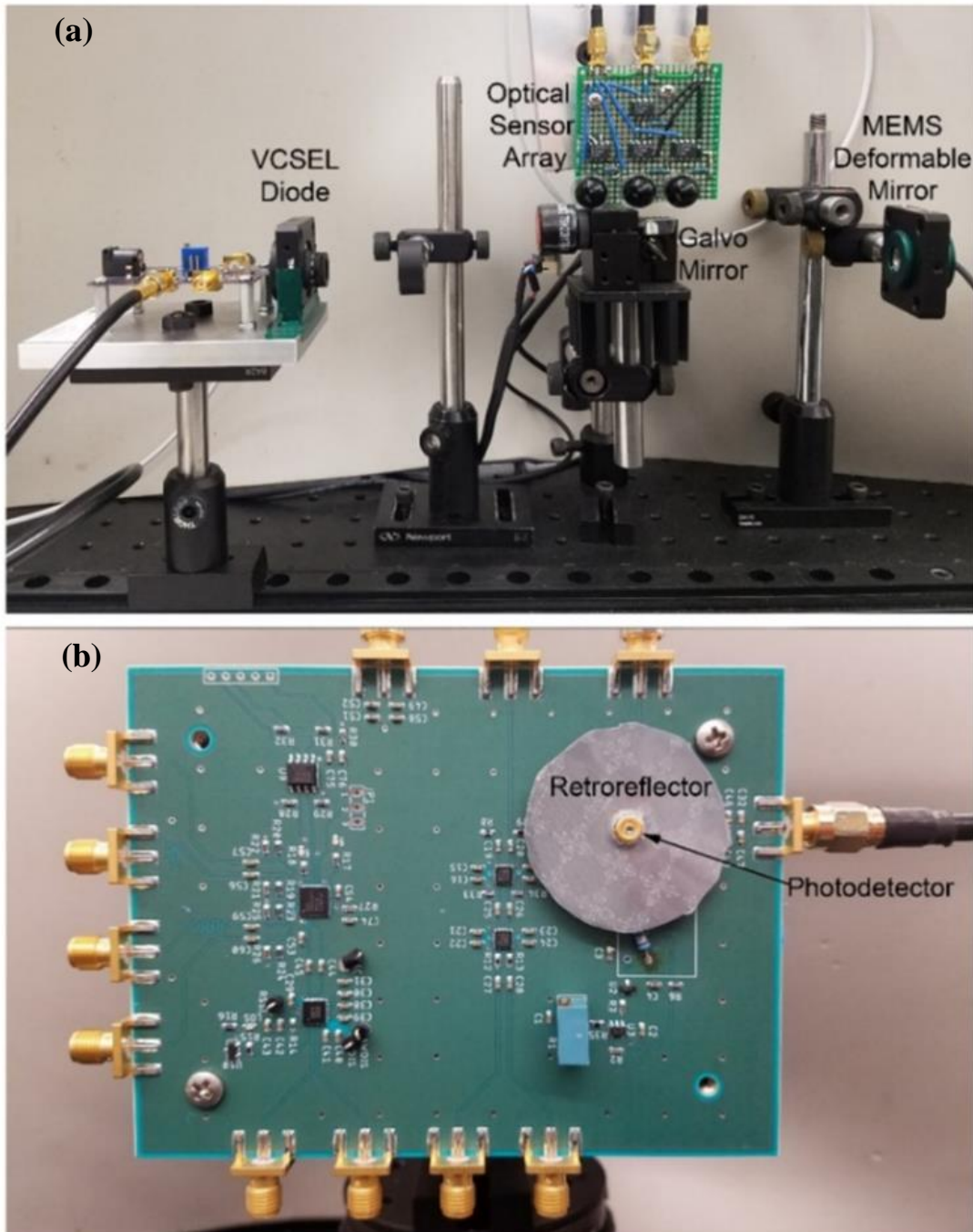
Figure 2.2: Photo image of the 850nm FSO system: (a) the transmitter module and the beam steering & beam shaping module; (b) the receiver module with a retroreflector as the passive beacon.

2.2.4 User Location Acquisition Algorithm

By pointing the beam at various locations and measuring the reflected signal using the optical sensor array, we can determine the angular position of the user in the FOV. Using a highly divergent beam to carry out this search increases the probability of striking the retroreflector, but it also makes the location measurement less accurate. This tradeoff implies that rapidly and precisely locating a user within the FOV requires a robust beam control algorithm, which we refer to as the user location acquisition algorithm.

A straightforward implementation of this algorithm is to sequentially scan the entire FOV with a fine angular resolution. While this approach would consistently and precisely locate a user, hardware limitations make it excessively slow. For example, scanning a ($\pm16°$, $\pm10°$) FOV with a $0.1°$ angular resolution generates 64,000 data points and takes at least 32 seconds using the 2 kHz scanning rate in the hardware described above. Alternatively, while scanning the entire FOV with a course angular resolution of $2°$ completes in a reasonable amount of time (< 1 sec), it lacks the location accuracy required to support high-speed communication with the receiver.

A more efficient approach, and the approach used in this article, is a three-step scanning algorithm. This approach divides user acquisition into three steps of progressively smaller sections of the FOV with progressively higher angular resolutions. This is only made possible by our combined beam steering and beam

shaping capability. Furthermore, we employ a hexagonal lattice scanning pattern to pack the Gaussian beams most efficiently in the FOV, minimizing the risk of missing the user. In order to explain this acquisition algorithm in more details, we define the following parameters that are also illustrated in Figure. 2.3 (a):

1) Scanning field-of-view (SFOV): this is the section of the total FOV scanned by the laser beam in each step.

2) Beam divergence angle (BDA): this is the divergence angle of the laser beam, which can be controlled by the deformable MEMS mirror. The value of the BDA is calibrated by the voltage applied to the control unit of the Revibro deformable MEMS mirror as discussed in Section 3.1.

3) Scanning angular resolution (SAR): this is the angular resolution of the hexagonal pattern created by the scanning laser beam. It is related to the angle between adjacent beam positions.

What follows is a step-by-step description of the three-step acquisition algorithm. An example of the scanning parameters is listed in Table.1:

Step I: Scan the entire FOV using a large BDA and SAR. The data acquired by the sensor array are processed to find the angular position of maximum reflection, which represents the approximate location of the retroreflector. This location is used as the center for the SFOV of Step II. Example Step I data are shown in Figure 2.3 (b).

Step II: Rescan the maximum reflection point of Step I with a smaller SFOV and BDA to more accurately determine the location of the retroreflector. Due to the better

SAR, the ring shape of the retroreflector can be identified in the reflection data, which we use to estimate the center of the retroreflector. However, the small size of the receiver's photodiode means that this estimation is still not sufficiently accurate to initiate high speed communicate with the user. Thus, this estimation merely serves as the center of the SFOV in Step III. Example Step II data are shown in Figure. 2.3 (c).

Step III: Rescan the retroreflector center found in Step II with an even smaller SFOV and SAR. Note that Step II is usually performed with the minimum BDA of our system (0.2°), so in this step we just increase the SAR and collect more data points around the center of the retroreflector. This leads to a reflection pattern with a large valley representing the location of the photodiode and gives a sufficiently accurate location measurement for high speed optical communication. Example Step III data are shown in Figure 2.3 (d).

To determine the position of the reflector from a scan, we compute the average position of all points deemed to be part of the retroreflector. For the first two scans, this means averaging the positions of points with reflection values above an experimentally determined threshold. For the third scan, which resolves the hole in the center of the retroreflector as seen in Figure. 2.3 (d), points below a certain threshold are included in the average. We need to point out that the size of the retroreflector should be further reduced in order to be integrated with mobile user electronic devices. The challenge associated with smaller retroreflectors comes from the weaker reflected optical beacon signals to locate the user in Step I scanning when the initial laser spot is relatively large.

Once the laser is focused, the impact of a small retroreflector is minimal. To address this problem, we can use a band-pass optical filter instead of a long-pass filter at the optical sensor array to further reduce the ambient light noise. In addition, we can use chopped optical signals with an electronic filter at the receiver to probe the retroreflector, which will significantly improve the signal-to-noise ratio.

The total time to locate the user using this hardware and the three-step acquisition algorithm is around 1.1~1.2 seconds. A breakdown of the scanning time required for each step is presented in Table 1. Note that the time required for data processing and hardware/software communication is negligible with respect to the scanning time.
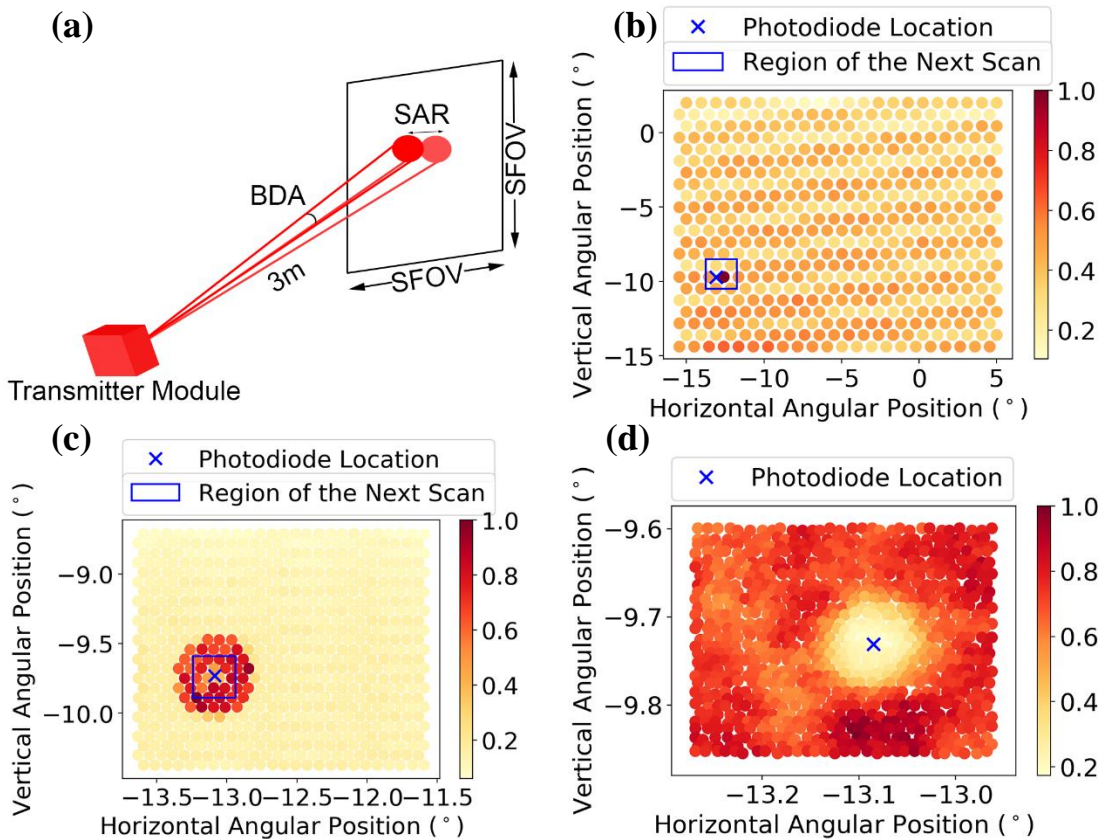
Figure 2.3: (a) Illustration of the parameters for the three-step scanning algorithm; (b)~(d) experimentally collected reflection patterns in the three scanning steps at 3-m distance. Note: the power is normalized for the calibration of different BDAs

TABLE I. PARAMETERS FOR THE THREE-STEP SCANNING ALGORITHM AND THE SCANNING TIME OF EACH STEP

	Step I	Step II	Step III
SFOV	$25° \times 25°$	$2.5° \times 2.5°$	$0.3° \times 0.3°$
BDA	$1.3°$	$0.2°$	$0.2°$
SAR	$1.125°$	$1°$	$0.0125°$
Scanning Time	0.354 sec	0.344 sec	0.481 sec

2.3 Experimental Results

2.3.1 Characterization of the Deformable MEMS Mirror

To guarantee reliable user location and optical communication, we experimentally determined the BDAs that result from different control voltages to the deformable mirror, and also ensured that optical signal quality is maintained when the optical beam is reflected by the mirror. The Revibro deformable beam shaping mirror is an electrostatic device that is driven by a four-channel high-voltage amplifier that maps a 0 to 5V analog input to a 0 to 400V analog output. These voltages correspond to a variable mirror focal length of $\infty \leq f \leq 67$mm and draw a range of power from 0 to

10mW to drive the input. Each of the four analog input channels controls one of the four concentric circular actuators located on the back of the reflective membrane mirror of the device. These channels can be tuned individually to reduce spherical aberrations or tied together for simplicity. The high-voltage amplifier provided by Revibro has a bandwidth of 25 kHz, and the reflective membrane mirror has a diameter of 4 mm and a settling time of 150μs. When 0 V is applied to the four inputs, the membrane is flat and forms a mirror with an infinitely long focal length. When 5 V is applied, the membrane is maximally deformed and creates a concave mirror with a focal length of 67 mm. The result of this deformation on the laser beam is shown in Figure 2.4 (a). These images, which were captured by an IR camera with a telescope lens, show the laser beam spot size projected on a piece of target paper when 0 V and 5 V are applied to the control inputs. As the input voltage increases, the mirror deforms and causes the beam to diverge. By measuring the beam's optical power at a range of control voltages, the BDA for each control voltage can be calculated with a simple geometry optics method. Using an optical power meter with a 1-mm aperture iris, we carried out this experiment at 1, 3, and 10 meters from the deformable mirror. Results are shown in Figure 2.4 (b). Note that the 1-meter results are slightly different than the 3 meter and 10-meter results, which is likely caused by the Fresnel diffraction of the near field pattern as the calculated Rayleigh range of the Gaussian beam is found to be 15 meters. Additionally, as the distance from the mirror increases, the calculated BDA shows

progressively larger variation, which could possibly result from the non-uniform beam profile or laser speckle, which is subject to further investigation.
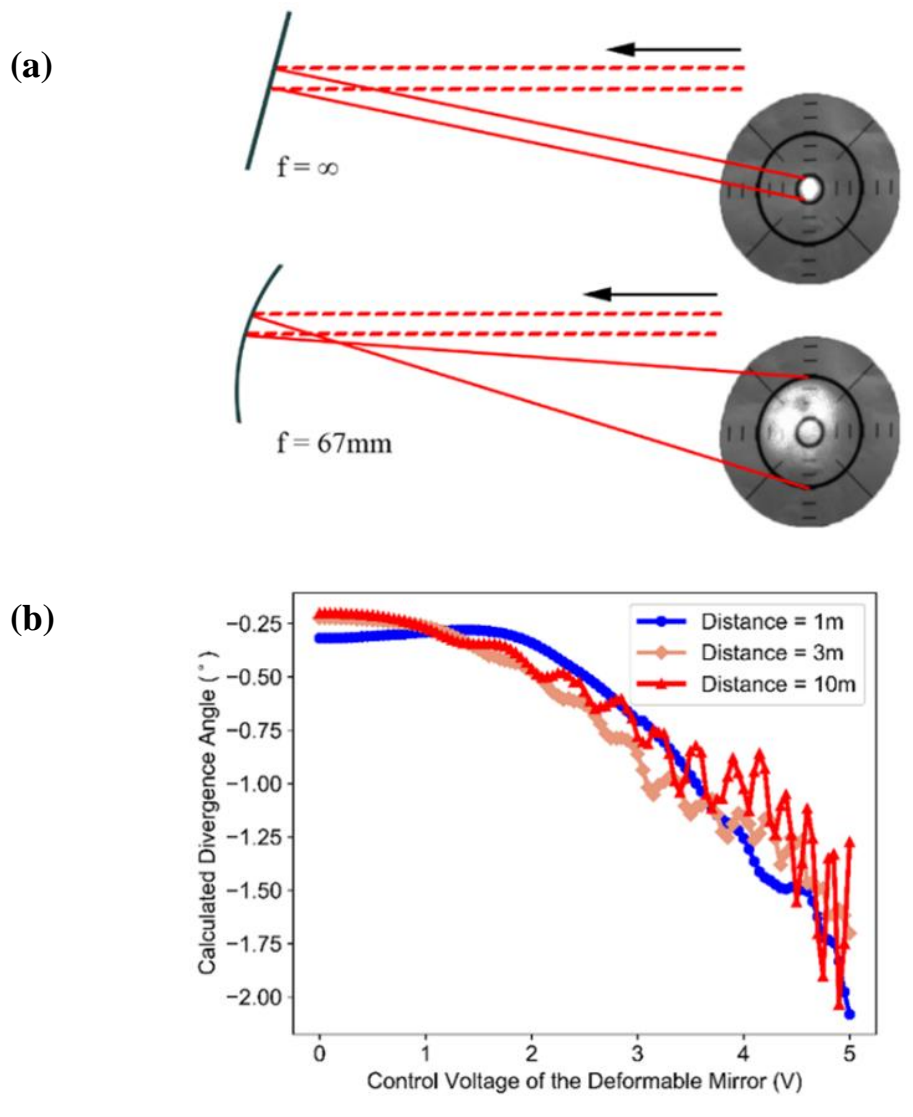
(a)

(b)

Figure 2.4: (a) Illustration of beam shaping using the Revibro deformable MEMS system; (b) Calculated BDA as a functional of the control voltages by measuring the received optical power density at different distances. The discrepancy of each measurement possibly comes from non-ideal Gaussian beam profile

To evaluate the effect of the deformable mirror to the optical signal integrity, we measured the eye diagrams of the received optical signals at a range of deformable mirror control voltages. This was done by placing an optical receiver 2 meters from the mirror in the center of the beam and varying the mirror deformation. Figure 2.5 (a) shows the eye diagrams for a 1 Gb/s optical signal at a 3 V and 0 V deformable mirror voltage. Clearly, a collimated beam with a small BDA provides better signal quality. A more quantitative measurement is shown in Figure 2.5 (b), which shows the Q-factor and optical modulation amplitude (OMA) as a function of the control voltage (bottom x-axis) as well as the diameter of the transmitted beam on the receiver plane (top x-axis). The diameter of the laser beam is minimized when the deformable mirror is flat resulting in the best collimated beam. As the mirror control voltage increases, the focal length of the beam is reduced and leads to larger beam divergence. When fully collimated, the transmitted laser beam has a diameter of 3.54mm on the receiver plane.

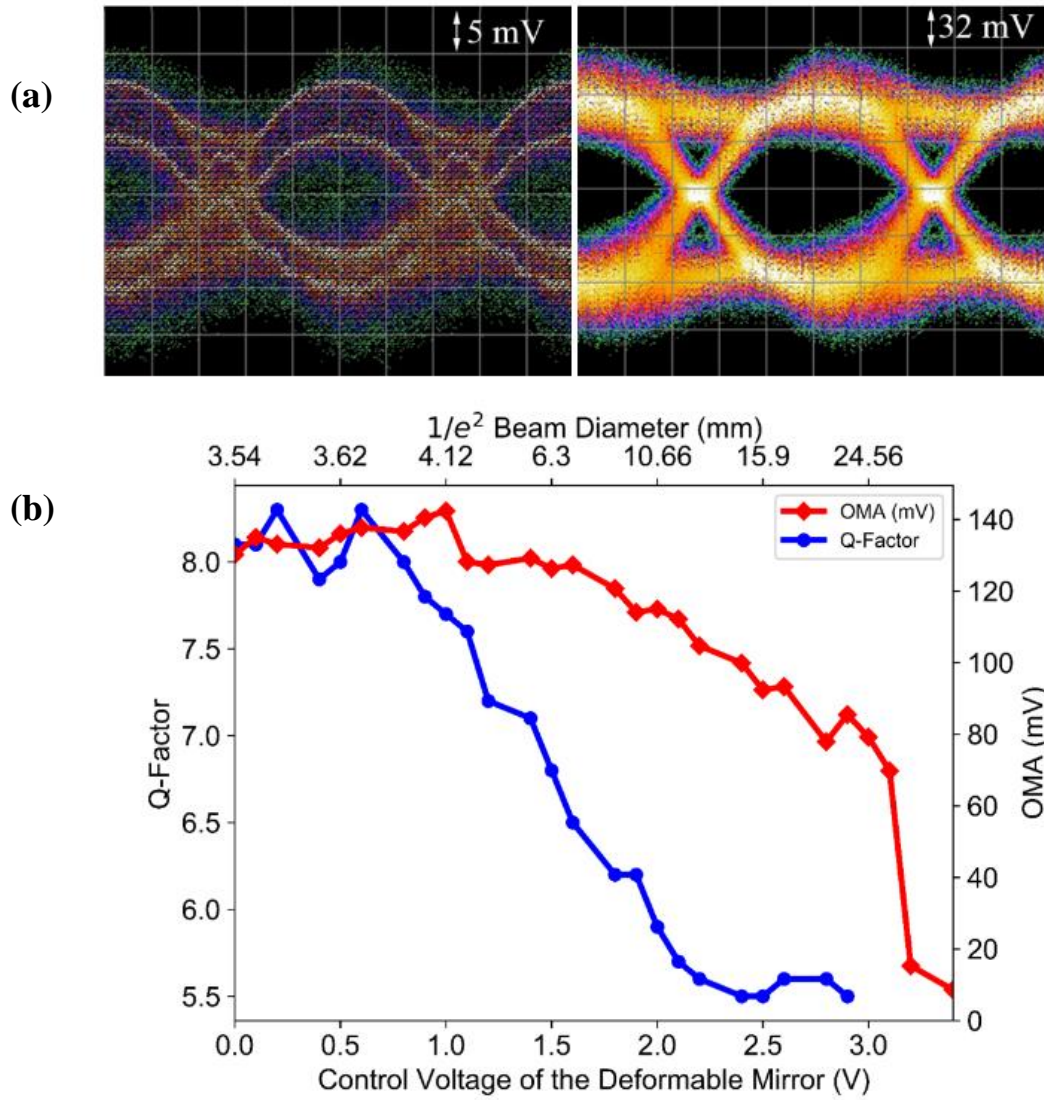Figure 2.5: (a) Eye diagrams of the received optical signals at 3V and 0V driving voltage to the deformable mirror; and (b) continuously measured Q-factor, OMA, and beam diameter of the received optical signal as a function of the control voltage as well as the diameter of the transmitted beam on the receiver plane. All results were measured at 2-m distance between the transmitter and receiver.

2.3.2 Characterization of the Agile FSO System

To characterize the entire FSO system as illustrated in Figure 2.1, the receiver module was placed at 80 different locations within the transmitter's FOV at a distance of 3 meters. Due to the spatial symmetry, our testing only covers the first quadrant of the FOV, namely, $0° < \theta_x < 18.75°$ in the horizontal direction and $0° < \theta_y < 11.25°$ in the vertical direction, resulting in a quadrant area of $0.6m^2$ or a total scan area of $2.4m^2$. Testing locations within the first quadrant were roughly distributed as a 10×8 grid with slight random deviations. Each testing point was sampled three times for a total of 240 trials. During each trial, 20 Gb of data were transmitted through the FSO channel at a data rate of 1Gb/s, resulting in a confidence level of 86.5% given a BER floor of 1×10^{-10}. A Pseudo Random Binary Sequence (PRBS)-15 pattern was generated for the measurement with a pattern length of 32767 bits. The Q-factor, OMA, and BER of the received optical signals and the scanning time of each trial were recorded. In terms of Q-factor, OMA and BER, our FSO system performs exceptionally well within the entire FOV as shown in Figure 2.6 (a)-(c). Usually the Q-factor of the eyes are correlated with the BER of the binary data. If Gaussian noise is assumed, the relationship can be quantized as $BER = \frac{1}{2}erfc(\frac{Q}{\sqrt{2}})$[37]. However, ideal Gaussian noise may not always exist and therefore, we included both Q-factor and BER results. Most sampled positions returned a BER of less than 1×10^{-9}, while the worst BER was just 4×10^{-7}, which can be easily compensated by standard error reduction techniques

such as forward error correction. The OMA heat map shown in Figure 2.6 (c) further demonstrates the quality of this link. With OMA from 90mV to 140mV, it leaves significant margin for noise suppression and tolerance to misalignment. A realtime video showing the successful user location with 1Gb/s data transmission by the agile FSO system is included as the Visualization file.
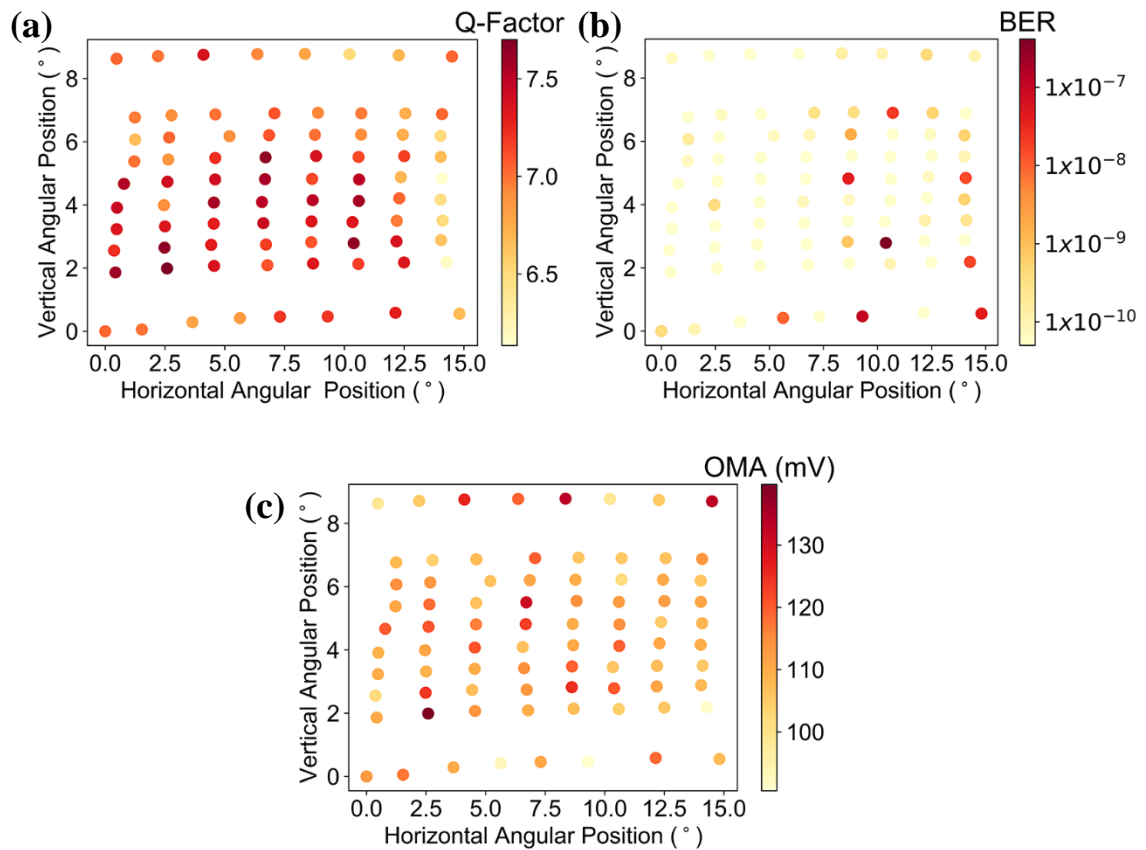

Figure 2.6: Angular distribution of the experimentally measured (a) Q-factor, (b) BER, and (c) OMA of the recevied optical signal within the FOV at 3-m distance.

The areal coverage of our system is mainly contrained by the galvo mirrors used for beam steering, which have a maximum deflection angle of ±25°. Extending the distance between the optical transmitter and the receiver can increase the covered area. However, this approach is limited by two factors. First, the best collimation of the laser beam is around 0.2° and longer communication distance will result in decreased power density at the receiver, which could increase the BER. Second, the angular resolution (0.01°) of the galvo mirrors may result in uncertainties of finding the user at longer distance. As shown Figure 2.6(b), some significantly increased BER data, although still below 10^{-6}, can be observed at the edges of the scan area, which is most likely casued by the repeatibility issue of beam steering close to the maximum angle. Considering a good receiver circuit can accept around 10mV OMA, we can still tolerate at least 10× smaller received optical power. This will translate into roughly 3x larger communication distance to 9 meters. The In future designs, we could increase the total covered area by selecting mirrors with larger steering angles, or we could propose a network consisting of multiple optical cells similar to the concept of RF wireless communication.

Histograms of the Q-factor, OMA and BER for all 240 trials are shown in Figure 2.7 (a)-(c) and demonstrate the consistency of this FSO system. Thus, this system is not only capable of establishing robust links, but the links are highly repeatable. Additionally, the data in the angular space distribution above shows no obvious bias toward any particular direction. Figure 2.7 (d) shows the histogram of the

total scanning time of each user location process, which is 1.17±0.06 seconds. The acquisition time of our system is currently limited by the mechanical movement of the beam steering device as listed in Table 1. The galvo mirrors that we use to direct the transmitted beam operate on a time scale of a few hundred hertz when scanning across their full ±25° scan range. This time scale is significantly slower than the deformable mirror (150μs settling time), the sampling ADC (5000s/s), or the execution time of the scanning algorithm (<1μs). A reduction in the overall system size and acquisition time is certainly possible by replacing the bulky, slow moving galvo mirrors with miniaturized MEMS beam steering mirrors [31], or even more advanced non-mechanical beam steering devices such as optical phased array devices [30], which may be implemented in future FSO systems. We also would like to point out that this relatively long acquisition time is only necessary when the transmitter seeks to initiate the first time connection with the user. Once the initial connection is established, we can use a continuous user tracking algorithm that we are currently developing to maintain a stable optical communication.
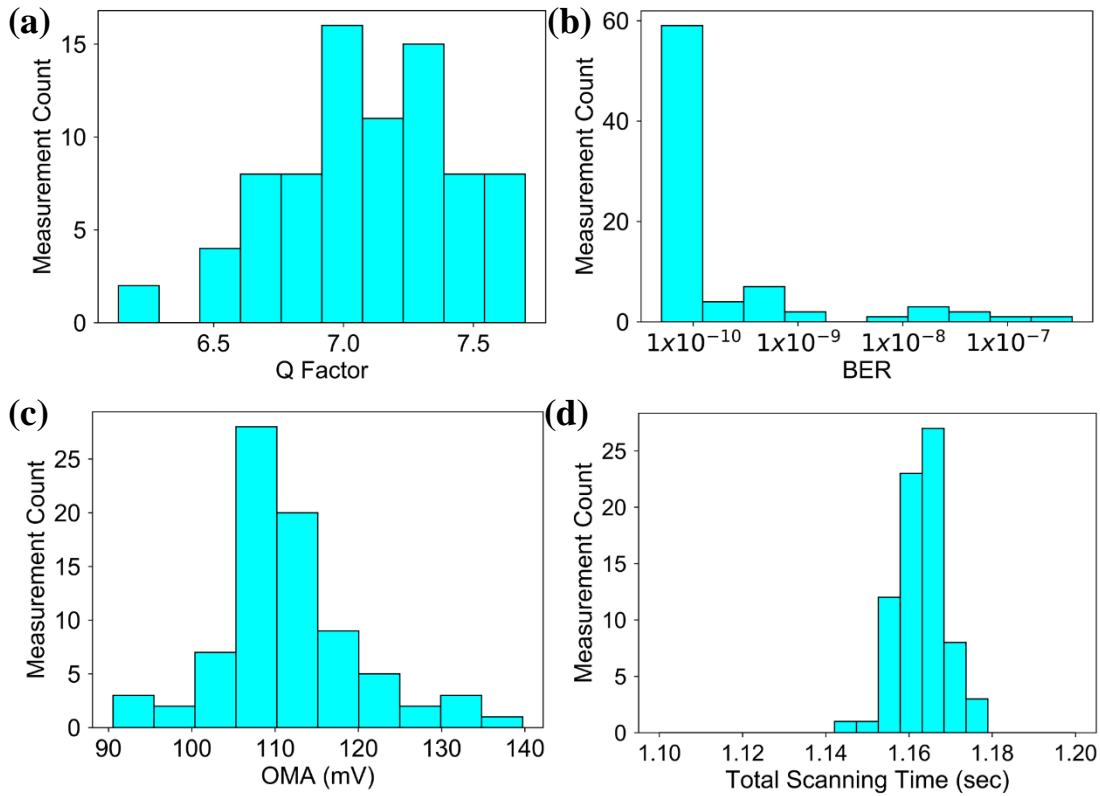
Figure 2.7: Histograms of the measurement count of the 240 trials measured at 3-m distance: (a) Q-factor, (b) BER, (c) OMA, and (d) total scanning time, which show satisfying repeatibility of the dynamic FSO system.

2.4 Conclusion

In summary, we presented an agile FSO link with beam steering and beam shaping capabilities for indoor wireless communication. The FSO system features an agile beam control system that can direct and shape an optical beam to establish reliable, LOS connection for any user location within the FOV. It can also adjust the

laser beam spot onto the user to enhance the received optical power and ensure data security. The FSO system consists of three primary components: a transmitter module using commercial low-power VCSEL diode, a beam control unit consisting of galvo-mirrors, a deformable MEMS mirror and an optical sensor array, and a receiver module with a ball-lens photodiode and a ring-shaped retroreflector. The ring-shaped retroreflector reflects the transmitted beam to the optical sensor array, allowing all-optical location of the user. The three-step scanning algorithm allows the transmitter to locate the receiver with millimeter-scale precision at a distance of 3 meters in approximately 1.16 seconds. The robustness of this FSO system was demonstrated by placing the receiver in 80 locations throughout the FOV and establishing a high-speed optical link with measured BERs consistently below 4×10^{-7}, requiring only 2 mW of optical power from the transmitter.

CHAPTER 3: Dynamic, 10Gb/s, Free-Space Optical Communication Enhanced by User Tracking Technologies

3.1 Background

The increasing bandwidth demands of kinetic users have garnered research interest for several decades. Research in minimizing vibrational loss in satellites has been demonstrated success by means of aperture optimization [38], and beam divergence optimization for active tracking and pointing systems [39]. Optical user location techniques have been developed using angle of arrival techniques [40], distribution of optical power triangulation techniques [41]. Research in augmented reality has provided insights into user tracking in the form of Kalman filter estimation of user location enabled by retroreflector markers [42], and blob extraction, two-dimensional prediction guided by IR retroreflector systems [43]. Prioritization of data transmission in kinetic communication requirements poses a significant challenge due to the fundamental tradeoff between sending data and gathering user location information. To address these trade-offs we propose a dynamical beam steering and shaping FSO system enabled by Kalman filter estimation.

3.2 System Architecture

As shown in Figure 3.1. the system makes use three key modules: the transmitter module, the beam controlling module, and the receiver module. The

transmitter module features an off-the-shelf CISCO SFP+ transceiver with data rates up to 10Gb/s. The collimated light from the SFP transmitter is modulated using an NRZ-OOK modulation scheme and sent to the beam controlling module. The beam controlling module makes use of beam steering and beam shaping via an off-the-shelf Thorlabs galvomirror and a Revibro Optics MEMS deformable mirror. When the light from the beam controlling module detects the retroreflector in the FOV, the optical sensor receives user location feedback, and transmits that data into the user tracking algorithm. The user tracking algorithm ensures that the beam controlling module directs the light to the receiver module in the FOV. The receiver module is comprised of a retroreflective tape toroidally wrapped around a high-speed off-the-shelf Kyoto Semiconductor PIN photodiode with an internal TIA. The transmitter is driven via a BERT and the overall system output from the receiving module transmits back to the BERT to establish a BER measurement.
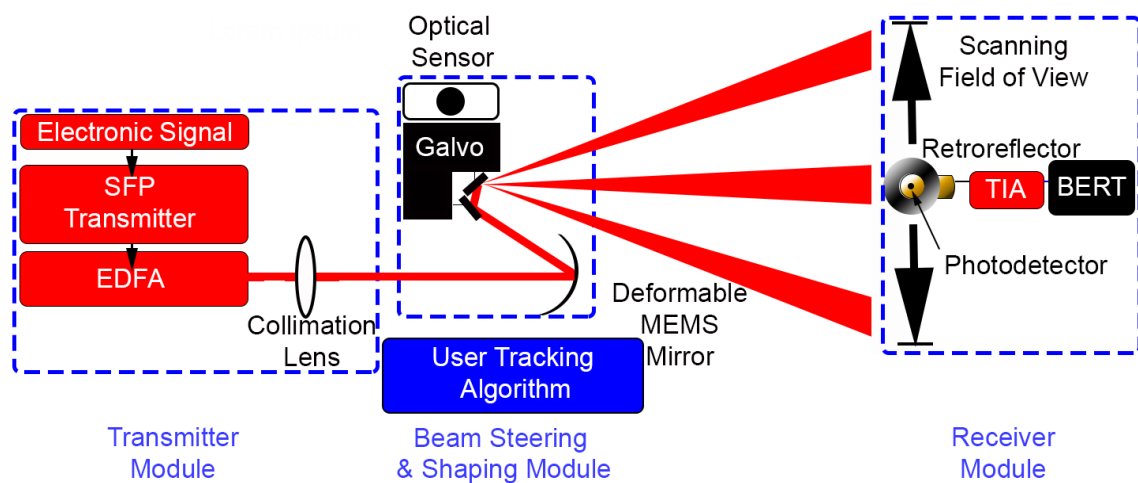
Figure 3.1: Schematic of the 1550nm user tracking FSO system consisting of a transmitter module, a beam steering and beam shaping module controlled by a user location tracking algorithm, and receiver module with a retroreflector.

3.2.1 Transmitter Module

The transmitter module is shown in Figure 3.5. An eye-safe, off-the-shelf CISCO transceiver with a center wavelength at 1550nm was chosen as the transmitter. The transmitter is then coupled into a Thorlabs collimation stage with a 10x magnification microscope lens is used to collimate the output light of the fiber connected to the SFP output. The use of 1550nm as a wavelength allows for the integration of an erbium doped fiber amplifier (EDFA) to drastically increase system performance. The system is further augmented with a Thorlabs polarization maintaining (PM) EDFA to increase the overall optical power of the system as seen in Figure 3.2
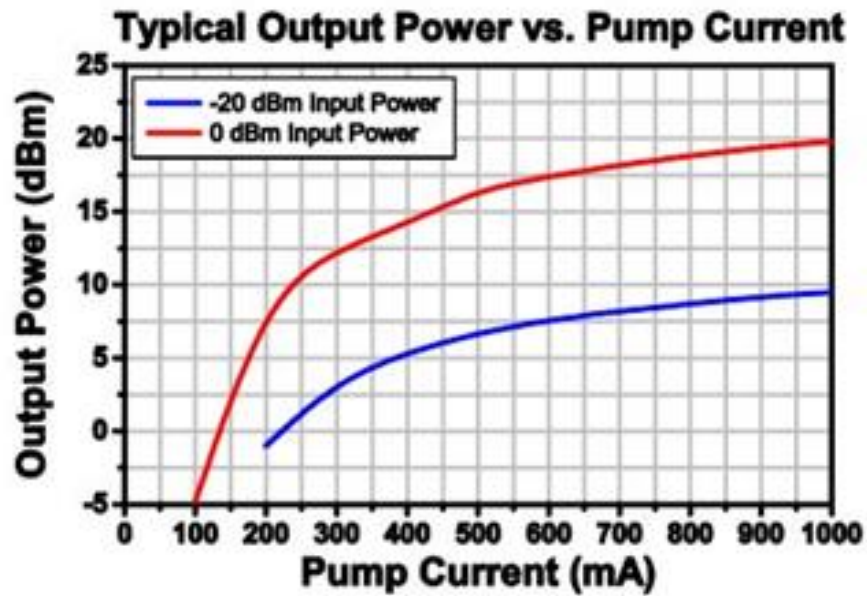
(a)

(b)

Figure 3.2: Thorlabs PM EDFA: (a) Image of Thorlabs EDFA; (b) Output power as a function of pump current. The output power plot is provided by Thorlabs.

3.2.2 Beam Controlling Module

The beam controlling module is also shown in Figure 3.5 The beam steering method comes from an off-the-shelf Thorlabs GVS-002 galvomirror. This mirror features a FOV of ±17° in the horizontal direction and ±25° in the vertical direction when used with an input beam of >4mm. The beam shaping technique comes from an off-the-shelf Revibro Optics deformable MEMS mirror. The MEMS mirror takes an input voltage of 0-5V and amplifies the signal to 0-400V across 4 electrostatically actuated regions. When these regions achieve maximum deflection, the variable focal length ranges from $-\infty < f \leq 67mm$. Included in the beam controlling module is an optical sensor comprised of a Thorlabs FGA21 photodiode with an active area of $3.1mm^2$ and a non-inverting amplified circuit. This sensor is filtered using a Thorlabs FEL0800 longpass filter with a cut-on wavelength of 800nm. This filter blocks out the visible light, while a 0.5in lens focuses the received signal into the sensor circuit.

3.2.3 Receiver Module

The receiver module, which is show in Figure 3.5., utilizes a uses an off-the-shelf Kyoto Semiconductor KPDX10G photodiode with an integrated TIA and a sensitivity of -18dBm. The photodiode is packaged into an ultracompact custom designed PCB with dimensions of 1.2in × 1.4in as seen in Figure 3.3:

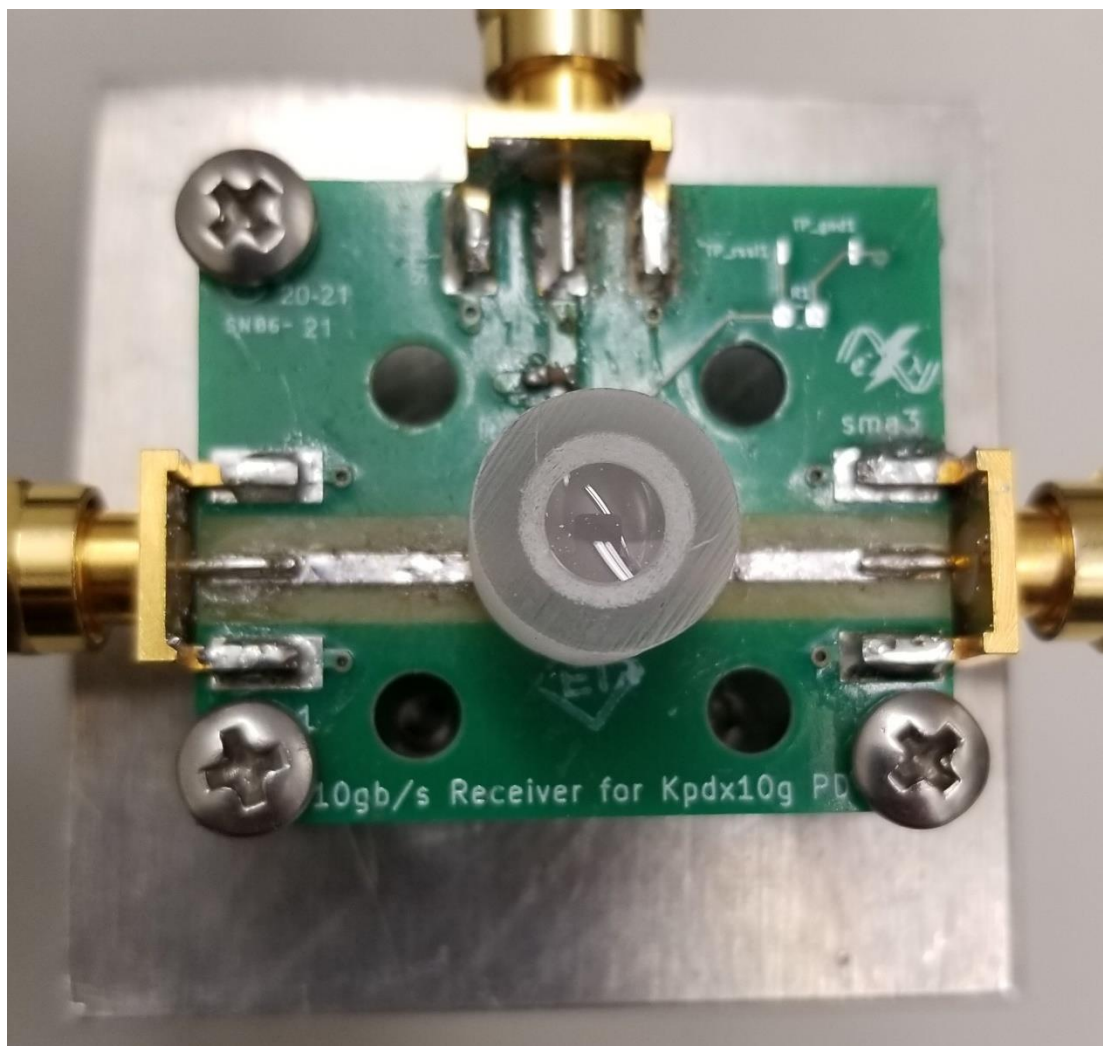Figure 3.3: Ultracompact receiver featuring KPDX10G photodiode adorned with an ink-jet printed lens.

Due to the telecom application of 1550nm and the fundamental tradeoff of bandwidth and active areas for photodiodes, the active region of the KPDX10G does not allow for direct free-space coupling into the photodiode. Such an active region is too small for free-space applications without the use of a lens. Leveraging the tradeoffs

between magnification and viewing angle a custom-made ink-jet printed lens system was designed and fabricated by Voxtel. These lenses can be seen in Figure 3.4:
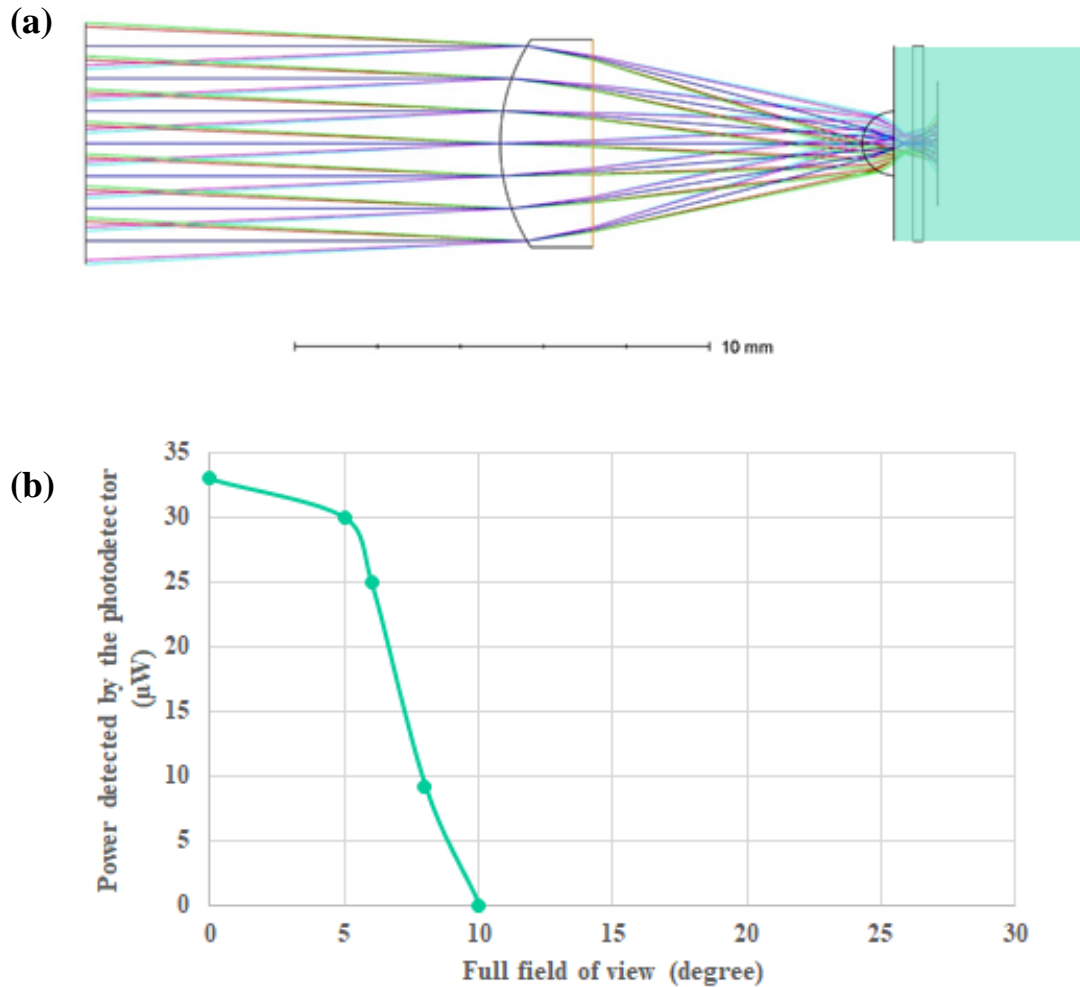
(a)

(b)

Figure 3.4: Voxtel lens details: (a) a Zemax rendering of the chromatic light paths taken and their interaction with the can photodiode; (b) the power as a function of viewing angle. Both the Zemax rendering, and the graph are generously provided by Voxtel.
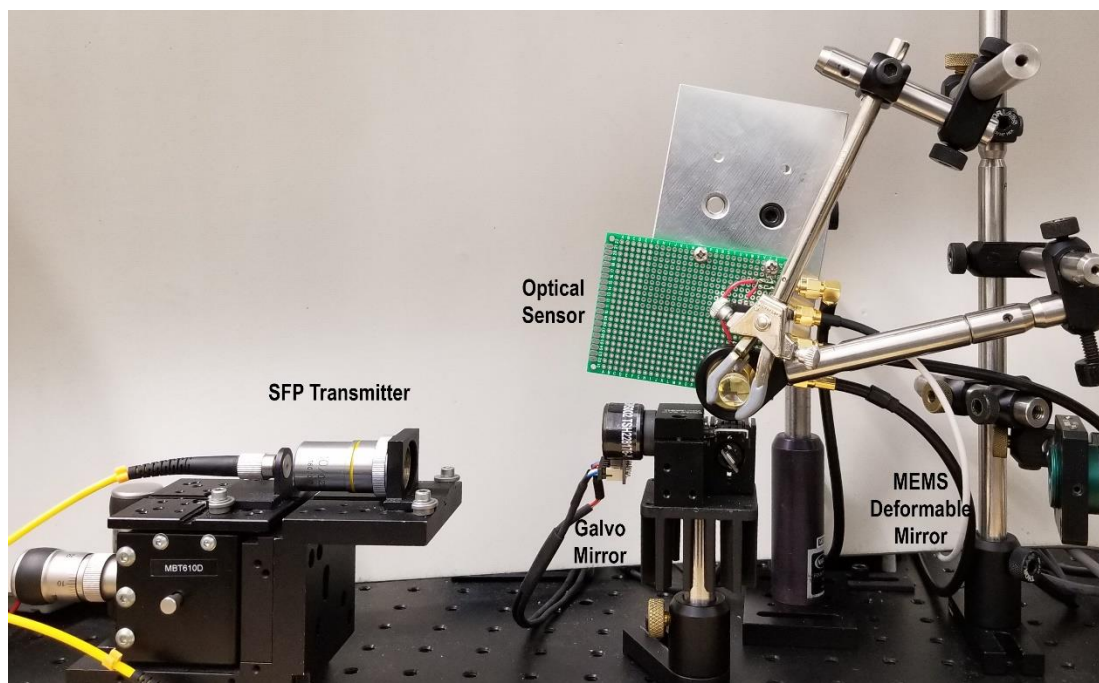
Figure 3.5: Photo image of the 1550nm FSO system with the transmitter module and the beam steering & beam shaping module.

3.2.4 User Tracking Algorithm

The user tracking algorithm developed by Luc Bouchard, utilizes the beam controlling module to rapidly scan the field of view to measure reflections from the retroreflector. The reflections are used in a Kalman filter to estimate the state of the user position. The duration of the scan is determined as a function of the SFOV, as such, minimizing the time to locate a user can be achieved by minimizing the scan area. Data from the Kalman filter is used in a Monte Carlo simulation in order to determine

the optimal scan area and repeatedly updated to ensure a constant lock with the user while minimizing time to scan, thus increasing the time spent transmitting data.

3.3 Experimental Results

Early experimental results have been achieved for the user tracking algorithm utilizing a legacy 850nm system. Initial results can be observed in Figure 3.6 where the mean squared error (MSE) for tracking can be observed as a function of velocity.
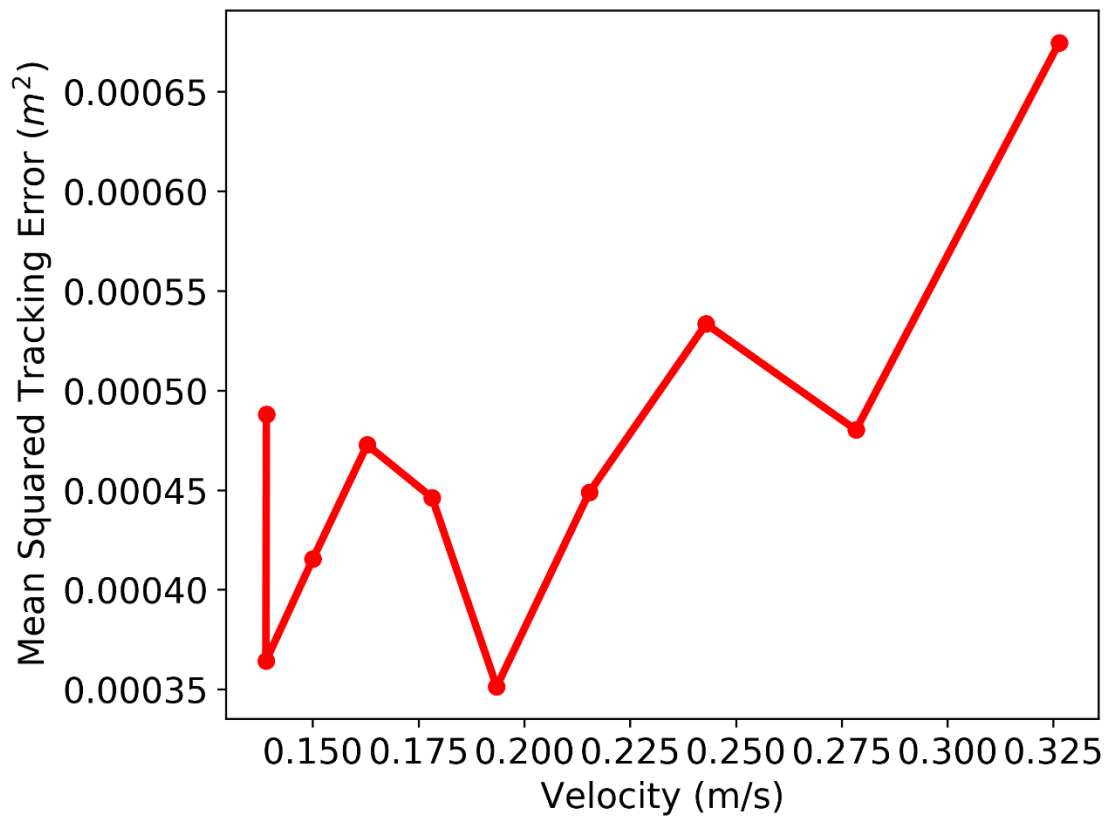
Figure 3.6: Mean squared tracking error as a function of velocity.

3.3.1 Characterization of the Communication Modules

To guarantee the optical performance of the system, a characterization of the CISCO SFP transmitter was conducted via an optical spectrum analyzer (OSA) as seen in Figure 3.7:
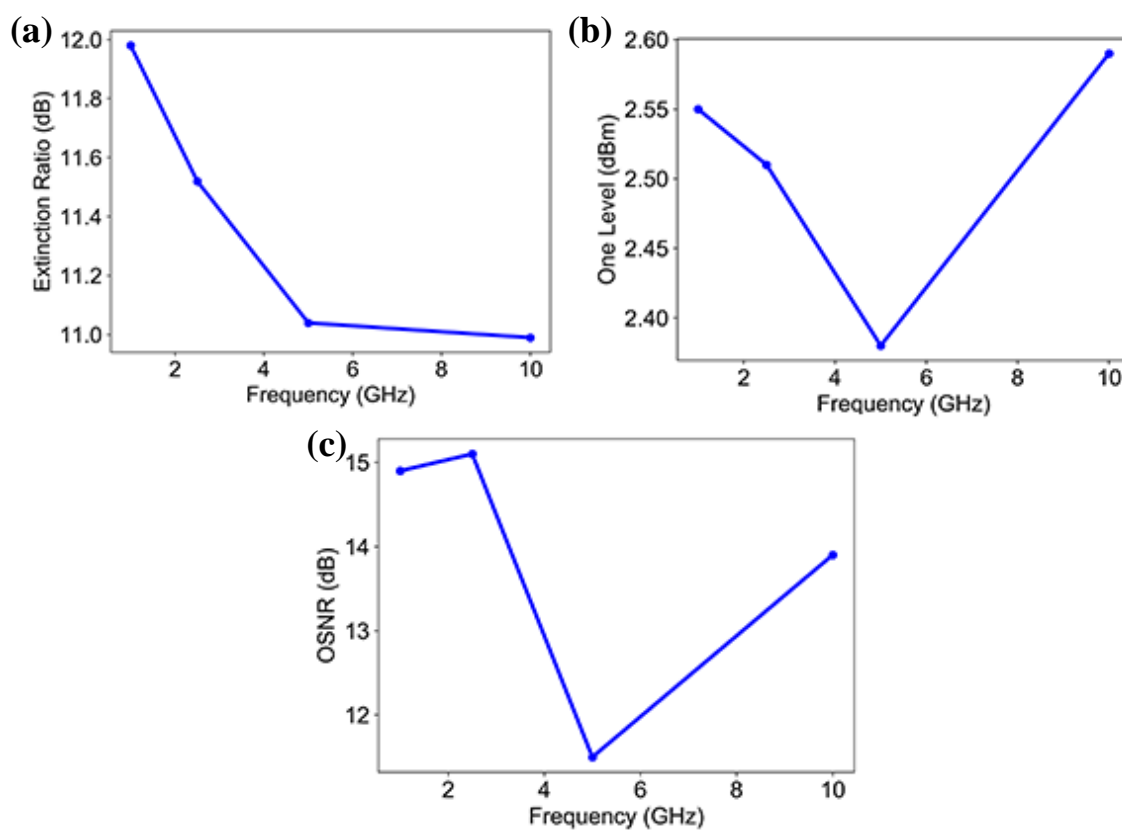
Figure 3.7: OSA characterization of the SFP transmitter: (a) Extinction ratio vs. frequency; (b) One level vs. frequency; (c) optical signal to noise ratio (OSNR) vs. frequency.

In order to ensure high BER communication between the SFP transmitter and the ultracompact receiver, several data rates were tested to ensure high-speed communication was possible within the 3m distance as seen in Figure 3.8:
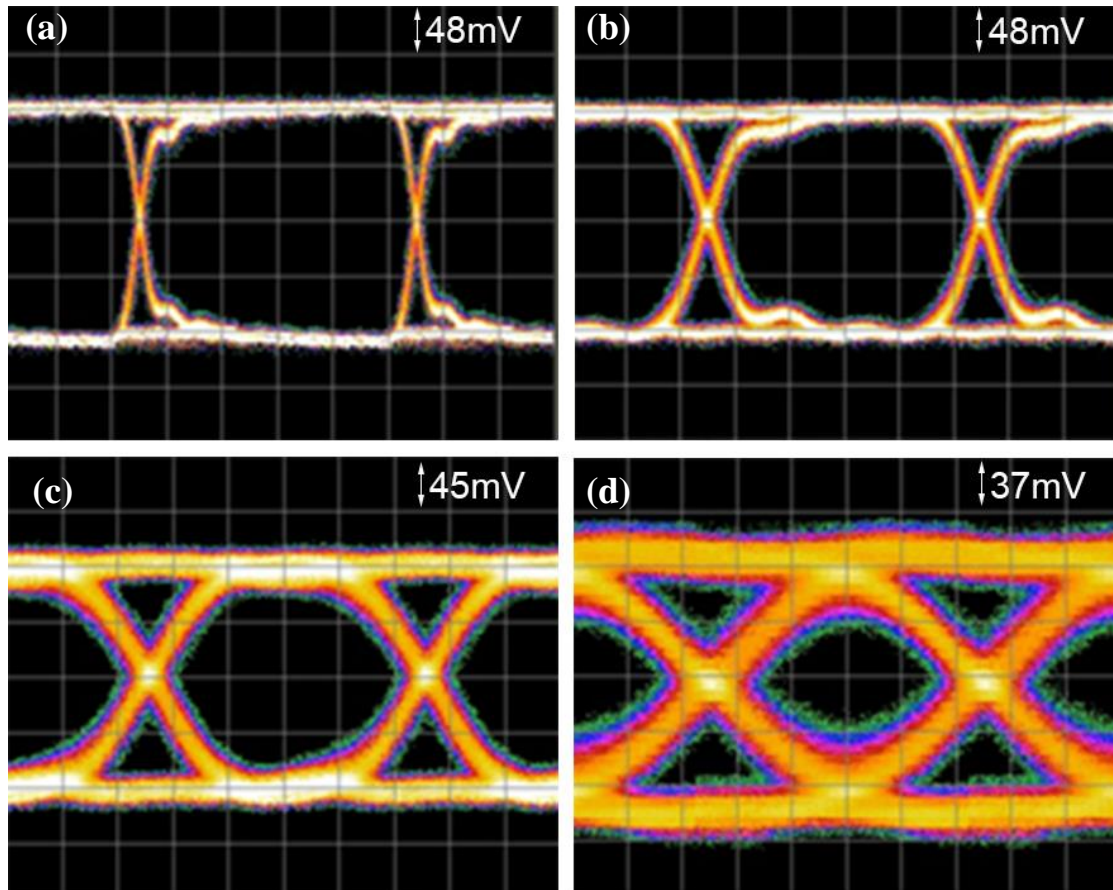
Figure 3.8: (a) 1GHz PRBS-15 on the KPDX10G. (b) 2.5GHz PRBS-15 on the KPDX10G. (c) 5GHz PRBS-15 on the KPDX10G. (d) 10GHz PRBS-15 on the KPDX10G.

The highest BER measured occurred at a driving frequency of 10GHz with a value of 4.96×10^{-7} which is within acceptable margins for forward error correction techniques.

3.4 Conclusion

In this chapter, a novel FSO system capable of delivering 10Gb/s data rates securely was proposed. Custom designed PCBs were fabricated and tested to fullfill the needs of optical sensing, and high-speed data receiving. Ink-jet lenses were designed and fabricated to increase SNR while leveraging angular acceptance requirements. The initial groundwork for the system shows promising results, but more work is needed to experimentally validate this system. Recent advancements in the tracking algorithm in the form of Monte Carlo simulations for optimal SFOV size will likely see an increase to the performance of these statistics.

CHAPTER 4: Conclusion

The necessity for innovation in high-speed data communication combined with advancements in free-space optical communications allow for the implementation of novel and robust FSO solutions. Our approach of dynamically adjustable beam steering and shaping uniquely addresses the needs for faster, safer, and more efficient FSO systems. The two systems proposed allow for indoor, high-speed, optical communications.

Although the first system was experimentally validated, the second still requires further system analysis and performance testing. Two key remaining measurements are: the root mean squared error of user location as a function of velocity for every location in the field of view, and BER as a function of user velocity.

Future improvements upon this system should include the introduction of Lissajous scanning to optimize the inertial movement of the scanning mirrors, thus increasing the scanning frequency, and electronic filtration/modulation of the beam searching for the retroreflector to drastically reduce the SNR of the system. Finally, the use of these systems in quantum key distribution networks yields the potential to add an additional layer of security upon an already critical area of research.

References

1. K. Kikuchi, , and C. Lorattanasane, "Compensation for pulse waveform distortion in ultra-long distance optical communication systems by using midway optical phase conjugator,". *IEEE photonics technology letters*, vol. 6, no.1, pp.104-105, 1994.

2. L. Long, G. Xie, Y. Ren, N. Ahmed, H. Huang, Z. Zhao, P. Liao et al. "Orbital-angular-momentum-multiplexed free-space optical communication link using transmitter lenses." *Applied Optics* vol. 55, no. 8, pp.2098-2103 2016.

3. R. K. Tyson, "Principles of adaptive optics*". CRC press*, 2015.

4. T. Komine, and M. Nakagawa, "Fundamental analysis for visible-light communication system using LED lights," *IEEE transactions on Consumer Electronics*, vol. 50, no.1, pp.100-107, 2004.

5. M.Z. Afgani, H. Haas, H. Elgala, and D. Knipp, "Visible light communication using OFDM". *In IEEE 2nd International Conference on Testbeds and Research Infrastructures for the Development of Networks and Communities*," pp.6, 2006.

6. P.H. Pathak, X. Feng, P. Hu, and P. Mohapatra, "Visible light communication, networking, and sensing: A survey, potential and challenges*," IEEE communications surveys & tutorials,* Vol.17, no.4, pp.2047-2077, 2015.

7. K. Cui, G. Chen, Z. Xu, R.D. Roberts, "Line-of-sight visible light communication system design and demonstration," *2010 IEEE 7th International Symposium on Communication Systems, Networks & Digital Signal Processing*, pp.621-625, 2010.

8. X. Wu, M.D Soltani, L. Zhou, M. Safari, and H. Haas, "Hybrid LiFi and WiFi networks: A survey," *arXiv preprint arXiv*:2001.04840, 2020

9. C.L. Tsai, and Z.F. Xu "Line-of-sight visible light communications with InGaN-based resonant cavity LEDs," *IEEE photonics technology letters*, Vol.25, no.18, pp.1793-1796, 2013.

10. A. Tsaitmas, C.P. Baggen, F.M. Willems, J.P.M. Linnartz, and J.W. Bergmans, "An illumination perspective on visible light communications," *IEEE Communications Magazine*, vol. 52, no.7, pp.64-71, 2014.

11. Z. Yu, R. J. Baxley, and G.T. Zhou, "Multi-user MISO broadcasting for indoor visible light communication," *IEEE International Conference on Acoustics, Speech and Signal Processing*, pp.4849-4853, 2013,

12. T.P. Nguyen, and A.X. Wang, "Increasing data bandwidth to wireless devices," U.S. Patent 9,831,954. 2017.

13. Q. Wang, T. Nguyen, and A.X. Wang, "Channel capacity optimization for an integrated wi-fi and free-space optic communication system (wififo)," *ACM Proceedings of the 17th ACM international conference on Modeling, analysis and simulation of wireless and mobile systems*, pp.327-330, 2014.

14. S. Liverman, Q. Wang, Y.J. Chu, A. Borah, S. Wang, A. Natarajan, A.X. Wang, and T. Nguyen, "A hybrid communication network based on integrated free-space optical and WiFi femtocells," *Computer Communications*, vol.132, pp.74-83, 2018.

15. T. Komine, and M. Nakagawa, "Integrated system of white LED visible-light communication and power-line communication," *IEEE Transactions on Consumer Electronics*, vol.49, no.1, pp.71-79, 2003.

16. S.W. Wang, F. Chen, L. Liang, S. He, Y. Wang X. Chen, and W. Lu, "A high-performance blue filter for a white-led-based visible light communication system," *IEEE wireless communications*, vol.22, no.2, pp.61-67, 2015.

17. C. Lee, C. Zhang, M. Cantore, R.M. Farrell, S.H. Oh, T. Margalith, J.S. Speck, S. Nakamura, J.E. Bowers, and S.P. DenBaars, "4 Gbps direct modulation of 450 nm GaN laser for high-speed visible light communication," *Optics express*, vol.23, no.12, pp.16232-16237, 2015.

18. S. Liverman, H. Bialek, A. Natarajan, A.X. Wang, "VCSEL array-based gigabit free-space optical femtocell communication," *Journal of Lightwave Technology*, vol.38, no.7, pp.1659-1667, 2019.

19. J.A. Simpson, B.L. Hughes, and J.F. Muth, "Smart transmitters and receivers for underwater free-space optical communication," *IEEE Journal on selected areas in communications*, vol.30, no.5, pp.71-79, 2012.

20. Z. Sodnik, B. Furch, and H. Lutz, "Optical intersatellite communication," *IEEE journal of selected topics in quantum electronics*, vol.16, no.5, pp.1051-1057, 2010.

21. H. Kaushal, and G. Kaddoum, "Optical communication in space: challenges and mitigation techniques," *IEEE communications surveys & tutorials*, vol.19, no.1, pp.57-96, 2016.

22. W.S. Rabinovich, C.I. Moore, R. Mahon, P.G. Goetz, H.R. Burris, M.S. Ferraro, J.L. Murphy, L.M. Thomas, G.C. Gilbreath, and M. Vilcheck, "Free-space optical communications research and demonstrations at the US Naval Research Laboratory," *Applied optics*, vol.54, no.31, pp.189-200, 2015.

23. S .S. Muhammad, T. Plank, E. Leitgeb, A. Friedl, K. Zettl, T. Javornik, and N. Schmitt, "Challenges in establishing free space optical communications between flying vehicles," *IEEE 6th international symposium on communication systems, networks and digital signal processing*, pp.82-86, 2008.

24. Y. Ren, G. Xie, H. Huang, N. Ahmed, Y. Yan, L. Li. C. Bao, M.P. Lavery, M. Tur, M.A Neifeld, and R. W. Boyd, "Adaptive-optics-based simultaneous pre- and post-turbulence compensation of multiple orbital-angular-momentum beams in a bidirectional free-space optical link," *Optica*, vol.1, no.6, p.376-382, 2014.

25. C. Hindman, and L. Toberton, "Beaconless satellite laser acquisition-modeling and feasibility," Proc. *IEEE Mil. Commun. Conf. (MILCOM)*, pp.41-4, 2004.

26. I. Toselli, L.C. Andrews, R.L. Phillips, and V. Ferrero, "Free-space optical system performance for laser beam propagation through non-Kolmogorov turbulence," *Optical Engineering*, vol. 47, no.2, pp. 026003, 2008.

27. N. A. Riza, "Reconfigurable optical wireless," *in Proc. IEEE Lasers Electro-Optics Soc. (LEOS) 1999 12th Annual Meeting*, vol. 1, pp. 70–71, 1999

28. C.W. Oh, Z. Cao, E. Tangdiongga, and T. Koonen, "Free-space transmission with passive 2D beam steering for multi-gigabit-per-second per-beam indoor optical wireless networks," *Optics express*, vol. 24, no.17, *pp.*19211-19227, 2016.

29. C. Chaintoutis, B. Shariati, A. Bogris, P. Dijk, C. Roeloffzen, J. Bourderionnet, I. Tomkos, and D. Syvridis, "Free space intra-datacenter interconnects based on 2D optical beam steering enabled by photonic integrated circuits," In *Photonics, vol.*5, no.3, pp.21, 2018.

30. C.V. Poulton, D. Vermeulen, E. Hosseini, E. Timurdogan, Z. Su, B. Moss, and M.R. Watts, "Lens-free chip-to-chip free-space laser communication link with a silicon photonics optical phased array," *Frontiers in Optics*, pp. FW5A-3, 2017.

31. P. Brandl, S. Schidl, A. Polzer, W. Gaberl, & H. Zimmermann, "Optical wireless communication with adaptive focus and MEMS-based beam steering". *IEEE Photonics Technology Letters*, vol.*25, no.*15, pp.1428-1431, 2013.

32. P. J. Marraccini, & N. A. Riza, "Smart multiple-mode indoor optical wireless design and multimode light source smart energy-efficient links," *SPIE J. of Optical Engineering*, vol.52, no.5, pp. 055001, 2013

33. N. A. Riza, "Digital MEMS CAOS camceiver and a user positioning and IR ID data monitoring system for indoor optical and RF wireless environments," *2018 International Conference on Optical MEMS and Nanophotonics (OMN)*, pp. 1-2, 2018.

34. D. Milovančev, N. Vokić, H. Hübel, and B. Schrenk, "Gb/s visible light communication with low-cost receiver based on single-color LED," *Journal of Lightwave Technology*, vol.38, no.12, pp.3305-3314, 2020.

35. T. Koonen, "Optical wireless systems: technology, trends and applications," *2017 European Conference on Optical Communication (ECOC)*, pp. 1-3, 2017.

36. T. Koonen, K. A. Mekonnen, F. Huijskens, N.Q. Pham, Z. Cao, and E. Tangdiongga, "Fully passive user localization for beam-steered high-capacity optical wireless communication system," *Journal of Lightwave Technology*. vol.38, no.10, pp. 2842-2848, 2020.

37. X. Wang, W. Jiang, L. Wang, H. Bi, and R. T. Chen, " Fully embedded board-level optical interconnects from waveguide fabrication to device integration," *Journal of Lightwave Technology*, vol.26, no.2, pp.243-250, 2008.

38. S. Arnon, S. Rotman, and N. S. Kopeika, "Optimum transmitter optics aperture for satellite optical communication," *IEEE Transactions on Aerospace and Electronic Systems*, vol.34, no.2, pp.590-596, 1998.

39. H. Kaushal, and G. Kaddoum, "Optical communication in space: Challenges and mitigation techniques," *IEEE communications surveys & tutorials*, vol.19, no.1, pp.57-96, 2016.

40. A. Arafa, S. Dalmiya, R. Klukas, and J. F. Holzman, "Angle-of-arrival reception for optical wireless location technology," *Optics express*, vol.23, no.6, pp.7755-7766, 2015.

41. Y. Y. Won, S. H. Yang, D. H. Kim, and S. K. Han, "Three-dimensional optical wireless indoor positioning system using location code map based on power distribution of visible light emitting diode," *IET Optoelectronics*, vol.7, no.3, pp.77-83, 2013.

42. K. Dorfmüller-Ulhaas, "Robust optical user motion tracking using a kalman filter," 2007.

43. M. Ribo, A. Pinz, and A. L. Fuhrmann, "A new optical tracking system for virtual and augmented reality applications," *IMTC 2001. Proceedings of the 18th IEEE Instrumentation and Measurement Technology Conference*, Vol. 3, pp. 1932-1936, 2001.